ORIGINAL PAPER

Nonstationary coastal flood hazard analysis

Yiming Jia[1] · Mehrdad Sasani[1]

Abstract
It is well known that the increase in coastal flood hazard is expected to continue due primarily to climate change. While, previous studies have advanced probabilistic approaches for estimating future coastal flood hazard, two seminal issues have received little attention: (1) sea level trend projections that arise as a consequence of climate change not being incorporated in nonstationary coastal flood frequency analysis and (2) traditional stationary approaches that estimate return periods are not suited for analysis of nonstationary water levels. In this paper, a regression approach for sea level rise estimation is proposed to detrend water levels. The peak-over-threshold approach is used to analyze the probabilistic behavior of detrended water levels via a generalized Pareto distribution. Two interpretations of return period—the expected waiting time until an exceedance event occurs and the time associated with the expected number of exceedance events equal to one—are elaborated in a nonstationary context. By incorporating the existing sea level trend projections and using two interpretations of return period, flood hazard curves with uncertainty (i.e., water levels vs. return periods) are developed to describe the probabilistic behavior of future coastal flood hazards. Two case studies are conducted: one for Boston, Massachusetts, and one for New York City, New York.

1 Introduction

Coastal flooding can damage the lower portions of buildings, their contents, and other infrastructure. An accurate estimate of future water levels is needed to facilitate flood-resistant design and performance evaluation (e.g., define the design flood level and estimate the performance of structures under coastal flooding). Traditional methods to analyze extreme coastal water levels are often based on the assumption that coastal water level time series are stationary (ST) (e.g., Coles 2001). However, rising sea levels contribute to

✉ Mehrdad Sasani
   sasani@neu.edu

   Yiming Jia
   jia.yim@northeastern.edu

[1] Department of Civil and Environmental Engineering, Northeastern University, Boston, MA, USA

coastal flooding, thereby invalidating this assumption (Tebaldi et al. 2012; Zervas 2013; Kopp et al. 2014; Vitousek et al. 2016; Ghanbari et al. 2019, 2021; Taherkhani et al. 2020; Baldan et al. 2022). The global sea level has been increasing over the past century (Church and White 2006; Cazenave and Llovel 2010; IPCC 2014; Hay et al. 2015). The rate of sea level rise (SLR) is anticipated to increase globally and regionally, particularly under green-house gas emission scenarios (Nicholls and Cazenave 2010; Parris et al. 2012; IPCC 2014; Kopp et al. 2014; Hall et al. 2016; Sweet et al. 2017; Taherkhani et al. 2020).

Several studies over the course of the past few decades have accounted for the impact of SLR in nonstationary (NS) coastal flood frequency analysis. Their methodologies can be classified into two types. One involves fitting NS probability distributions to water level data, where the parameters of the NS probability distributions are modeled as functions of time (e.g., Katz et al. 2002; Mudersbach and Jensen 2010; Obeysekera and Park 2013; Obeysekera and Salas 2014; Salas and Obeysekera 2014; Luke et al. 2017; Razmi et al. 2017; Ghanbari et al. 2019, 2021; Baldan et al. 2022). The impact of SLR is implicitly and statistically incorporated in the parameters of the NS probability distribution. Flood hazard curves (water levels vs. return periods) are developed by extrapolating the parameter functions of the NS probability distribution into the future. Note that this extrapolation is valid only if water level trends remain the same. However, sea level trend projections are likely to show an acceleration (Nicholls and Cazenave 2010; Parris et al. 2012; IPCC 2014; Kopp et al. 2014; Hall et al. 2016; Sweet et al. 2017), which can affect the probabilistic behavior of water levels in the future. As such, the estimated functions for NS probability distribution parameters are anticipated to change, rendering flood hazard curves developed using extrapolation idealized and unlikely to be practical. The other methodology involves detrending water levels (removing the SLR trend), and then fitting ST probability distributions to the detrended water level data (e.g., Kirshen et al. 2008; Menéndez and Wood-worth 2010; Tebaldi et al. 2012, 2021; Zervas 2013; Sweet et al. 2014, 2022; Taherkhani et al. 2020). An ST probability distribution is defined by parameters that are fixed (time independent). In this methodology, the nonstationarity is accounted by the detrended SLR. The limitation of this methodology is that the concept of return period (RP) in an NS context is not considered. The developed flood hazard curves are only to report an RP for a given water level at a specific time, which is obtained from the fitted ST probability distribution and an estimated SLR.

The water level data for coastal flood frequency analysis is usually collected by one of two methods: annual maximum series and peak-over-threshold (POT). An annual maximum series is constructed using the highest recorded water level value for each year, which means that the sample size is equal to the number of years of data. The primary advantages of the annual maximum series method are its simplicity and the independence of extracted extremes (Tabari 2021). However, using only one data point per year will exclude potentially useful information, as there might be more than one large recorded water level in a year relative to other years' maxima (Lang et al. 1999; Bezak et al. 2014; Tabari 2021). An alternative to the annual maximum approach, the POT method, has been widely used in recent coastal flood frequency analyses (e.g., Tebaldi et al. 2012, 2021; Zervas 2013; Bezak et al. 2014; Ramzi et al. 2017; Talke et al. 2018; Ghanbari et al. 2019, 2021; Taherkhani et al. 2020). The POT method consists of retaining all peak water level values above a certain truncation level, usually referred to as the threshold (Lang et al. 1999). Thus, the POT method is not limited to one data point per year and allows for a more rational selection of extreme events. The main challenges of the POT method are choosing an appropriate threshold value and assuring the independence of threshold-exceeding data (Bezak et al. 2014). The appropriate threshold can be selected via multiple approaches, including

mean excess plot (e.g., Davison and Smith 1990; Lang et al. 1999; Coles 2001; Bommier 2014; Ramzi et al. 2017) and average number of over-threshold events (e.g., Lang et al. 1999; Nadal-Caraballo et al. 2016). The independence of threshold-exceeding data can be satisfied by using physical bases to set the time interval between peaks (e.g., Lang et al. 1999; Méndez et al. 2006; Nadal-Caraballo et al. 2016; Ghanbari et al. 2019, 2021). For threshold-exceeding data, a generalized Pareto distribution (GPD) is commonly used to model its probabilistic behavior (e.g., Davison and Smith 1990; Stedinger et al. 1993; Lang et al. 1999; Coles 2001; Méndez et al. 2006; Eastoe and Tawn 2010; Katz 2013; Silva et al. 2014; Nadal-Caraballo et al. 2016; Ramzi et al. 2017; Salas et al. 2018; Baldan et al. 2022; Pan et al. 2022).

The primary goal of this paper is to develop a methodology for NS coastal flood frequency analysis that produces flood hazard curves that can provide a complete probabilistic account for future coastal flood hazards. This involves (1) estimating SLR to detrend water level data, (2) using the POT method to estimate the probabilistic behavior of detrended water levels, (3) incorporating the existing sea level trend projections in RP calculation, and (4) describing the NS behavior of RPs. Critical features of this paper that distinguish it from previous studies are (1) incorporation of sea level trend projections, which arise from the consequences of climate change, in frequency analysis, and (2) consideration of the impact of NS behavior of RPs in flood hazard curve development. This methodology is applied to two case studies using water level data recorded by National Oceanic and Atmospheric Administration (NOAA) stations (NOAA 2023) near Boston, Massachusetts, and New York City, New York.

2 Methodology

In this section, the methodology for NS coastal flood frequency analysis that produces flood hazard curves is presented. This methodology includes SLR estimation, POT analysis for detrended water levels, annual exceedance probability estimation, and return period calculation incorporated with sea level trend projection.

2.1 Sea level rise estimation

Analogous to NOAA (2023), the existing SLR trend is estimated using monthly mean sea levels recorded by NOAA stations. It is worth noting that regular seasonal fluctuations from coastal ocean temperatures, salinity, wind, atmospheric pressure, and ocean currents are removed from the monthly mean sea levels (NOAA 2023). The estimated SLR is used to detrend recorded water levels during coastal floods, as described in the next section. Analogous to Obeysekera and Park (2013), Goddard et al. (2015), Nadal-Caraballo et al. (2016), Razmi et al. (2017), Baldan et al. (2022), Sweet et al. (2022), and NOAA (2023), the SLR trend is estimated by linear regression as

$$y = \beta_0 + \beta_1 \bullet t + \varepsilon \qquad (1)$$

where y is the sea level; t represents the recorded time; β_0 and β_1 are the regression intercept and slope; and ε represents regression residuals, which are assumed to be normal, homoscedastic (equality of variances), and independent (no serial correlation). However, based on the case studies shown in Sect. 3 (Results and Discussions), neither parametric (e.g., ordinary and weighted least squares) nor nonparametric (e.g., Theil-Sen (Theil 1950))

estimators can yield the homoscedastic and independent residuals from the Breusch-Pagan test (Breusch and Pagen 1979) and correlogram (Serago and Vogel 2018). One way to mitigate the heteroscedasticity of regression residuals is through data transformation (Helsel et al. 2020). Since, the SLR is estimated linearly, data transformation of time is accomplished by dividing Eq. (1) by t on each side:

$$\frac{y}{t} = \beta_0 \bullet \frac{1}{t} + \beta_1 + \frac{\varepsilon}{t} \tag{2}$$

Denoting $\frac{1}{t}$ as $t\prime$, and $\frac{y}{t}$ as $y\prime$, Eq. (2) can be rewritten as

$$y' = \beta_0 \bullet t' + \beta_1 + \varepsilon' \tag{3}$$

where ε' (equal to $\frac{\varepsilon}{t}$) is homoscedastic. To address the presence of serial correlation in ε', Helsel et al. (2020) recommend grouping the data into time intervals and computing a summary statistic for the interval, such as mean or median, and then using these summary statistics in the regression. This is suggested because the dependence that exists in ε' is an indication of considerable redundancy in the data (Helsel et al. 2020). In this paper, the mean values of sea levels at six-month intervals are used for regression.

2.2 Peak-over-threshold analysis for detrended water levels

A common practice when using the POT method is to remove the trend in the extreme dataset and then fit the probability distribution of the detrended extremes (e.g., Kirsten et al. 2008; Zervas 2013; Sweet et al. 2014, 2022; Nadal-Caraballo et al. 2016). The estimated SLR trends are used to detrend the hourly water levels recorded at the NOAA stations, which are obtained from tide gauges that measure the water level with respect to a local, fixed reference point on land. As such, these hourly water levels include (in addition to the SLR and local vertical land motion) astronomical tide height, storm surge height, and limited wave setup (FEMA 2007). The detrended hourly water levels are calculated as

$$z = z_t - (\beta_0 + \beta_1 \bullet t) \tag{4}$$

where z_t is the hourly water level recorded at time t; β_0 and β_1 are obtained by Eq. (3). These detrended hourly water levels are used in frequency analysis.

The peaks of the detrended hourly water levels (extreme values) that are above an appropriate threshold need to meet the independence condition as a prerequisite for frequency analysis and the Poisson process assumption (e.g., Davison and Smith 1990; Lang et al. 1999; Nadal-Caraballo et al. 2016; Ramzi et al. 2017). In this paper, the independence condition is defined from both a physical and statistical perspective. From a physical standpoint, Nadal-Caraballo et al. (2016) proposed to meet the independence condition of historical extreme water levels for the POT method by imposing a two-day time interval from the end of one storm to the start of the next. Note, that this imposed time interval does not define the time between peaks, which would be larger than two days. In this paper, a three-day time interval between peaks is selected to meet the independence condition, which is also recommended by Méndez et al. (2006), Sweet et al. (2014), Ghanbari et al. (2019), and Ghanbari et al. (2021). For a statistical approach, a correlogram (Serago and Vogel 2018) is used to evaluate the independence of peaks of detrended hourly water levels above the selected threshold (hereinafter referred to as POT water levels).

2.2.1 Threshold selection

In the POT method, it is important to select an appropriate threshold – one that is high enough to meet the model assumptions that the POT water levels are independent and the occurrence process can be described as a Poisson process. One commonly used method to select a threshold is interpreting the mean excess plot, also known as the mean residual life plot (e.g., Davison and Smith 1990; Lang et al. 1999; Coles 2001; Bommier 2014; Ramzi et al. 2017; Pan et al. 2022). A mean excess plot shows the threshold versus the mean value of threshold-exceeding peaks, which is

$$\frac{1}{n_u} \sum_{i=1}^{n_u} (x_i - u) \tag{5}$$

where u is the threshold, x_i is the i POT water level larger than u, and n_u is the number of POT water levels larger than u. If the GPD provides a valid approximation of the POT water levels larger than u, the mean excess plot should be approximately linear (Davison and Smith 1990; Lang et al. 1999; Coles 2001; Bommier 2014; and Ramzi et al. 2017). In addition to the mean excess plot, the average number of over-threshold events can provide guidance for threshold selection (Lang et al. 1999).

2.2.2 Generalized Pareto distribution

A GPD is used to model the probabilistic behavior of the POT water levels. The cumulative distribution function of the GPD for a given POT water level value is

$$F_X(x) = 1 - \left[1 + \xi \left(\frac{x - u}{\sigma} \right) \right]^{-\frac{1}{\xi}} \tag{6}$$

where $F_X(x)$ is the probability of the POT water level (X) not exceeding a given value (x); and ξ, σ, and u are shape, scale, and threshold (also known as location) parameters, respectively. If an NS trend exists in the POT water levels (e.g., estimated using linear regression), two methods can be used to incorporate the NS trend in the GPD parameter estimation:

1) Derive the moments of the POT water levels conditioned on time, such as by modeling the mean (conditioned on time) as a linear regression. Then, estimate the GPD parameters using these conditional moments via the method of moments. Examples can be found in Salas et al. (2018). Serago and Vogel (2018), Hecht and Vogel (2020), and Hecht et al. (2022). The uncertainty of GPD can be quantified using the prediction bounds of the conditional moments of the POT water levels.

2) Model the GPD parameters and/or their transformations (e.g., exponential, logarithmic) as functions of time. Then, estimate each of these parameters using the maximum likelihood method. Examples can be found in Coles (2001), Obeysekera and Park (2013), Salas and Obeysekera (2014), and Ramzi et al. (2017). The uncertainty of GPD can be calculated using the confidence bounds of GPD parameters.

If there is an ST trend in the POT water levels, it indicates that the GPD parameters are time independent. These parameters can be estimated using several approaches, such as the method of moments and the maximum likelihood method. More details about parameter estimation can be found in Hosking and Wallis (1987).

2.3 Annual exceedance probability

In the POT method, assuming that the occurrence of events follows a Poisson process, the exceedance probability of an event for a given time interval can be estimated using a GPD (e.g., Davison and Smith 1990; Cole 2001; Méndez et al. 2006; Eastoe and Tawn 2010; Katz 2013; Salas et al. 2018; Pan et al. 2022). The probability that the POT water level exceeds a given value during a time interval (ti) is calculated using the total probability rule:

$$P_{ti}(X > x) = 1 - \sum_{n=0}^{\infty} P(X \leq x|n) \bullet p_{ti}(n) \tag{7}$$

where $P(X \leq x|n)$ is the conditional probability that the POT water level (X) does not exceed a given value (x) for n water levels, which can be expressed as

$$P(X \leq x|n) = [P(X \leq x)]^n = \left[F_X(x)\right]^n \tag{8}$$

and $p_{ti}(n)$ is the probability that n POT water levels are observed during ti which is a rare event. Analogous to Davison and Smith (1990), Katz et al. (2002), Eastoe and Tawn (2010), Katz (2013), Bezak et al. (2014), Bommier (2014), Jia and Sasani (2021), Baldan et al. (2022), $p_{ti}(n)$ is assumed to follow a Poisson distribution

$$p_{ti}(n) = \frac{\lambda^n \bullet \exp(-\lambda)}{n!} \tag{9}$$

where λ is the recurrence rate, also known as the average number of over-threshold events. For the Boston and New York City cases, $\lambda = 1.70$ and 2.33, respectively. With ti defined as one year, the annual exceedance probability of X larger than x can be calculated

$$P_A(X > x) = 1 - \sum_{n=0}^{\infty} \left\{ \left[F_X(x)\right]^n \bullet \frac{\lambda^n \bullet \exp(-\lambda)}{n!} \right\} \tag{10}$$

Using Maclaurin series (Zwillinger 2012), Eq. (10) can be simplified as

$$P_A(X > x) = 1 - \exp\left\{-\lambda \bullet \left[1 - F_X(x)\right]\right\} \tag{11}$$

2.4 Return periods

The concept of RP is widely used to describe the occurrence of natural hazards, such as flood, wind, and earthquake. In this paper, RP is used to develop flood hazard curves under ST and NS conditions. Under the assumption of stationarity, RPs can be computed easily because the time to the next exceedance of a particular event follows a geometric distribution with a constant success probability. The RP is simply the inverse of the exceedance probability of the event of interest (Read and Vogel 2015). Under nonstationarity, however, the probabilistic behavior of RPs is much more complicated because the RP no longer follows a geometric distribution with a constant success probability. In fact, with even slightly NS behavior, the probability distribution of an RP looks nothing like a geometric distribution with a constant success probability, as shown by Read and Vogel (2015). Computing RP in an NS context

requires a prediction of flood events for the selected future time span along with a careful uncertainty analysis.

Within both ST and NS contexts, an RP can be interpreted as 1) the expected waiting time until an exceedance event occurs, denoted as RP_1 (Olsen et al. 1998; Cooley 2013; Cheng et al. 2014; Salas and Obeysekera 2014; Obeysekera and Salas 2014, 2016; Read and Vogel 2015; Salas et al. 2018; Naseri and Hummel 2022) or 2) the time associated with the expected number of exceedance events equal to one, denoted as RP_2 (Olsen et al. 1998; Parey et al. 2007, 2010; Cooley 2013; Obeysekera and Salas 2014, 2016; Read and Vogel 2015; Salas et al. 2018). The interpretation and computation of RP in the ST and NS contexts are elaborated below.

2.4.1 Return periods under stationarity

In an ST context, the sea level is assumed not to change in the future. RP_1 for a given water level follows a geometric distribution with a probability mass function of

$$f_{RP_1}(rp_1) = \left[1 - P_A(X_T > x_t)\right]^{rp_1-1} \bullet P_A(X_T > x_t) \tag{12}$$

where $P_A(X_T > x_t)$ is the annual exceedance probability that water level (X_T) exceeds a given value (x_t). X_T is equal to the POT water level $(X$, which is detrended) in relation to a sea level at a time of interest. Since sea level is assumed not to change in the future, $P_A(X_T > x_t)$ is consistent and equal to $P_A(X > x)$. RP_1 can be calculated as

$$RP_1 = \sum_{rp_1=1}^{\infty} rp_1 \bullet f_{RP_1}(rp_1) = \frac{1}{P_A(X_T > x_t)} \tag{13}$$

For RP_2, the number of exceedance events (E) follows a binomial distribution with probability mass function given by

$$f_E(e) = \binom{RP_2}{e} \bullet \left[P_A(X_T > x_t)\right]^e \bullet \left[1 - P_A(X_T > x_t)\right]^{RP_2-e} \tag{14}$$

The expected value of E is

$$E[E] = \sum_{e=1}^{\infty} e \bullet f_E(e) = RP_2 \bullet P_A(X_T > x_t) \tag{15}$$

Setting the expected value of E equal to 1, RP_2 can be calculated as

$$RP_2 = \frac{1}{P_A(X_T > x_t)} \tag{16}$$

Note, that the two interpretations of RP are identical in the ST context (see Eqs. (13 and 16)).

2.4.2 Return periods under nonstationarity

Under NS conditions, the sea level is assumed to be NS in the future. The probability mass function of RP_1 in an NS context can be written as

$$f_{RP_1}(rp_1) = \left\{ \prod_{i=1}^{rp_1-1} \left[1 - P_A(X_T > x_t|i)\right] \right\} \bullet P_A(X_T > x_t|rp_1) \tag{17}$$

where $P_A(X_T > x_t|i)$ and $P_A(X_T > x_t|rp_1)$ are the annual exceedance probabilities that X_T exceeds x_t in year i and rp_1, respectively. This can be calculated as $P_A(X > x)$ in relation to the corresponding sea levels in year i and rp_1, respectively. In other words, $P_A(X_T > x_t)$ is time-dependent. Analogous to Olsen et al. (1998), Cooley (2013), Cheng et al. (2014), Salas and Obeysekera (2014), Obeysekera and Salas (2014), Read and Vogel (2015), Obeysekera and Salas (2016), Salas et al. (2018),), and Naseri and Hummel (2022), Eq. (17) can be simplified as

$$RP_1 = \sum_{rp_1=1}^{\infty} rp_1 \cdot f_{RP_1}(rp_1) = 1 + \sum_{rp_1=1}^{\infty} \prod_{i=1}^{rp_1} [1 - P_A(X_T > x_t|i)] \tag{18}$$

For RP_2, E is expressed as

$$E = \sum_{i=1}^{RP_2} I(X_T > x_t|i) \tag{19}$$

where I is the indicator function. I is equal to 1 when X_T exceeds x_t in year i. Conversely, I is equal to 0 if X_T is less than or equal to x_t in year i. According to Cooley (2013), the expected value of E can be calculated as

$$E[E] = \sum_{i=1}^{RP_2} E[I(X_T > x_t|i)] = \sum_{i=1}^{RP_2} P_A(X_T > x_t|i) \tag{20}$$

Setting the expected value of E equal to 1, RP_2 in an NS context can be calculated numerically by solving

$$1 = \sum_{i=1}^{RP_2} P_A(X_T > x_t|i) \tag{21}$$

Note, that if there is an NS trend in the POT water levels, $F_X(x)$ and, in turn, $P_A(X > x)$ are not time independent. As such, two sources of nonstationarity (i.e., NS trends in both sea levels and POT water levels) need to be incorporated into the calculation of $P_A(X_T > x_t|i)$.

2.5 Sea level trend projection incorporation

As discussed above, computing RP in an NS context requires a prediction of flood events for the selected future time span along with a careful uncertainty analysis. From a statistical standpoint, two characteristics of flood events in the future need to be predicted–probabilistic behavior of the POT water levels discussed in Sect. 2.2.2 (Generalized Pareto distribution) and sea level trend. Considering the future sea level trend has been well studied, in this paper, the existing sea level trend projections with uncertainty (e.g., Yin et al. 2009; Kopp et al. 2014; Sweet et al. 2017, 2022) are incorporated in the RP calculation under NS condition.

3 Results and discussions

The proposed methodology for NS coastal flood frequency analysis is applied to two case studies using the NOAA recorded water level data near Boston, Massachusetts, and New York City, New York (NOAA 2023). The NOAA station locations in Boston Harbor, Massachusetts, and New York Battery Bay, New York are shown in Fig. 1. The
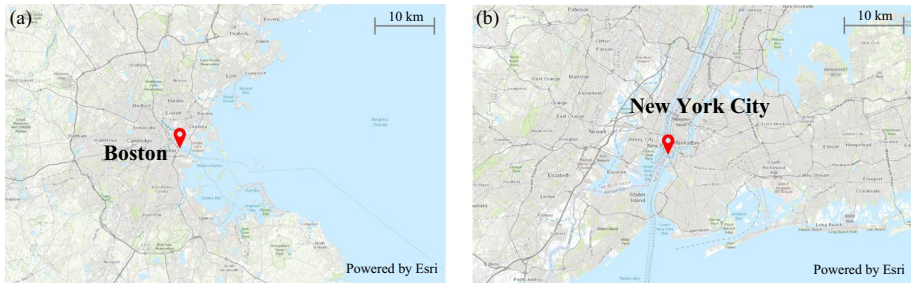
Fig. 1 NOAA water level station locations near **a** Boston and **b** New York City. (Map data from Esri |
USGS, NOAA, Tiles © Esri — Source: Esri, i-cubed, USDA, USGS, AEX, GeoEye, Getmapping, Aero-
grid, IGN, IGP, UPR-EGP, and the GIS User Community)

stations' information is shown in Table 1. For Boston, monthly mean sea levels (for
SLR estimation) and hourly water levels (for POT analysis of detrended water levels)
have the same record range. However, for New York City, the records for monthly mean
sea levels begin in 1856 but are incomplete between 1879 and 1892. The records for
hourly water level for New York City start in 1927. To be consistent with the frequency
analysis for the Boston case, the SLR for the New York City case is estimated using the
monthly mean sea levels from 1927 to 2022. All the water level data presented in this
paper uses the North American Vertical Datum of 1988 as a benchmark.

3.1 Sea level rise

The estimated β_1, i.e., the slope in Eq. (1), and the statistics of the estimated SLR trends
for Boston and New York City obtained via the ordinary least squares method are shown
in Table 2. In both cases, the p-value for the estimated β_1 is less than the 5% significance
level. Accordingly, the null hypothesis that there is an ST trend in sea levels is rejected.
ε' is normal, homoscedastic, and independent (see the regression residual analysis in
Appendix 5.1). The estimated sea levels and corresponding 95% prediction intervals are
shown in Fig. 2.

Table 1 NOAA water level station information

Location	Station ID	Latitude	Longitude	Record range for both monthly mean sea levels and hourly water levels
Boston	8,443,970	42° 21.2' N	71° 03.0' W	1921 ~ 2022
New York City	8,518,750	40° 42.0' N	74° 00.9' W	1927 ~ 2022

Table 2 β_1 and the statistics of the estimated SLR trends

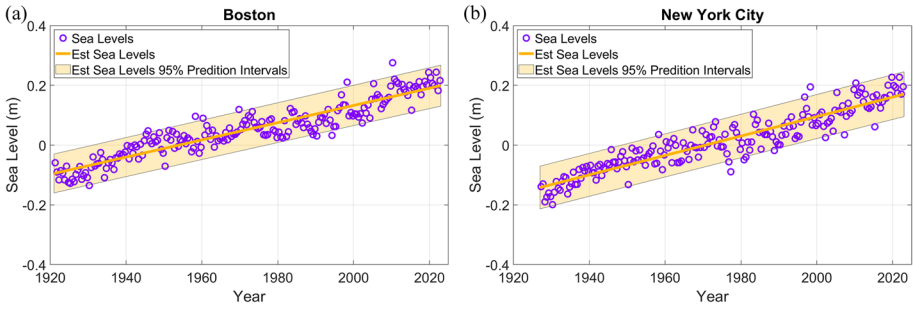| Location	Estimated β_1	p-value	Diagnostic result	Standard deviation of ε'
Boston	0.00288 m/yr (2.88 mm/yr)	< 0.001	ST trend is rejected	0.00017 m/yr (0.17 mm/yr)
New York City	0.00325 m/yr (3.25 mm/yr)	< 0.001	ST trend is rejected	0.00018 m/yr (0.18 mm/yr)

Fig. 2 Estimated sea levels and corresponding 95% prediction intervals developed using ordinary least squares estimators. **a** Boston and **b** New York City

3.2 Probability behavior of the peak-over-threshold water levels

For the Boston and New York City cases, the mean excess plots are shown in Fig. 3. According to Davison and Smith (1990), large fluctuations observed at high threshold values are the result of sampling variation in the data extremes and are not significant in determining the threshold (i.e., threshold values higher than 2.38 and 1.63 m for the Boston and New York City cases, respectively). In Fig. 3, the linearized portion of the mean excess plots (preceding the large fluctuations) are generated using the method outlined in Joyner et al. (2022). Similar to Davison and Smith (1990) and Ramzi et al. (2017), the thresholds are selected to equal the starting point of the last linear segment (i.e., $u = 2.04$ m and 1.19 m for the Boston and New York City cases, respectively). The developed correlograms (Fig. 11) in Appendix 5.2 illustrate that the selected POT water levels meet the independence condition.

In addition to the mean excess plot, the average number of over-threshold events can provide guidance for threshold selection (Lang et al. 1999). For the Boston and New York City cases, the average numbers of over-threshold events (using $u = 2.04$ m and 1.19 m) are 1.70 and 2.33, respectively. These average numbers of over-threshold events are comparable with those estimated by Nadal-Caraballo et al. (2016) – 1.50 and 2.00. The difference is due primarily to differing independence conditions (three days between peaks vs. two days between the ends of one storm to the start of the next used by Nadal-Caraballo et al. 2016) and the use of different threshold selection methods (mean excess plot vs. the
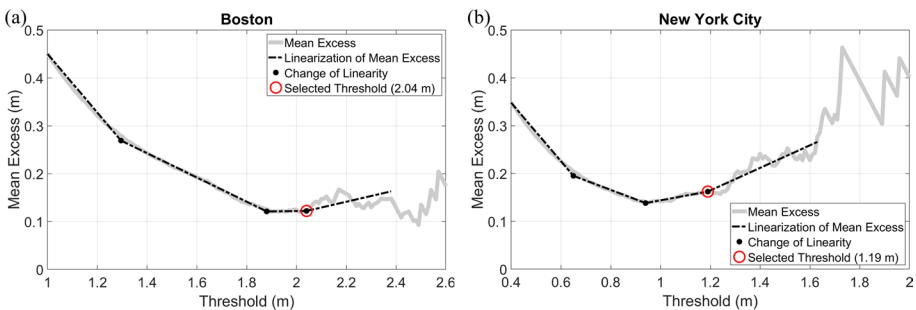

Fig. 3 Mean excess plots **a** Boston and **b** New York City

quantile–quantile optimization method used by Nadal-Caraballo et al. 2016). Using Eqs. (11 and 13), the RPs resulting from the selected threshold and corresponding average numbers of over-threshold events under ST condition are 1.22- and 1.12-year for the Boston and New York City cases, respectively, which are comparable to the RPs discussed in Lang et al. (1999)–1.15-year and 1.20- to 2.00-year.

To evaluate, whether there is an NS trend in the POT water levels, which can affect the following probability distribution fitting, a linear regression is fitted to the POT water levels. Figure 4b shows an outlier for the New York City case resulting from Hurricane Sandy in 2012. To mitigate the effect of outliers, Theil-Sen (Theil 1950) estimators – which, in contrast with ordinary least squares estimators, are not overly sensitive to outliers (Helsel et al. 2020)–are used to fit the linear trend in the POT water levels. For both the Boston and New York City cases, the p-values for the estimated β_1, i.e., the slope in Eq. (1), are higher than the 5% significance level (see Fig. 4). Therefore, the ST trend in the POT water levels is not rejected.

A GPD is used to model the probabilistic behavior of the POT water levels. Since, the ST trend in the POT water levels is not rejected, it is reasonable to assume that the GPD parameters are time independent. These parameters can be estimated using several approaches, such as the method of moments and the maximum likelihood method. More details about parameter estimation can be found in Hosking and Wallis (1987). For both the Boston and New York City cases, the method of moments fits the POT water levels better than the maximum likelihood method does. As such, the method of moments is used in this paper. The quantile–quantile plots between the POT water levels and those estimated via the method of moments are shown in Fig. 5 using the Gringorten plotting position (Gringorten 1963) as recommended by Kim et al. (2008). The Pearson correlation coefficient (ρ) between the POT water levels and the estimated POT water levels is used as a measurement for goodness-of-fit (see Fig. 5).

3.3 Sea level trend projection with uncertainty

Since, there is an ST trend in the POT water levels, it is reasonable to assume that the probabilistic behavior of the POT water levels in the future remains constant (see Fig. 4). Thus, only one characteristic of flood events in the future–sea level trend projection – needs to be estimated. Three sea level trend projections between 2000 and 2200 estimated by Kopp et al. (2014) are used for flood event prediction in this paper. These
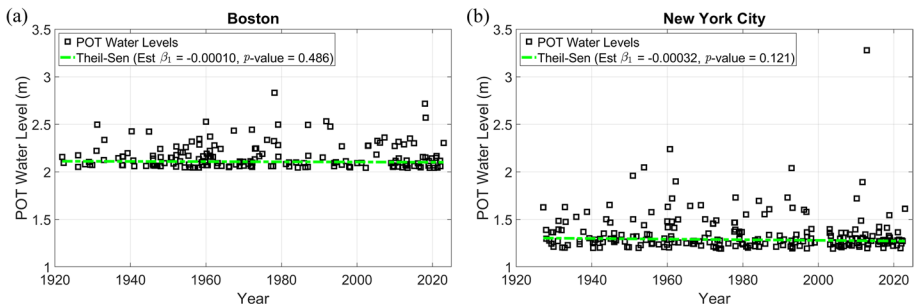

Fig. 4 Linear trends of the POT water levels developed using Theil-Sen estimators. **a** Boston and **b** New York City
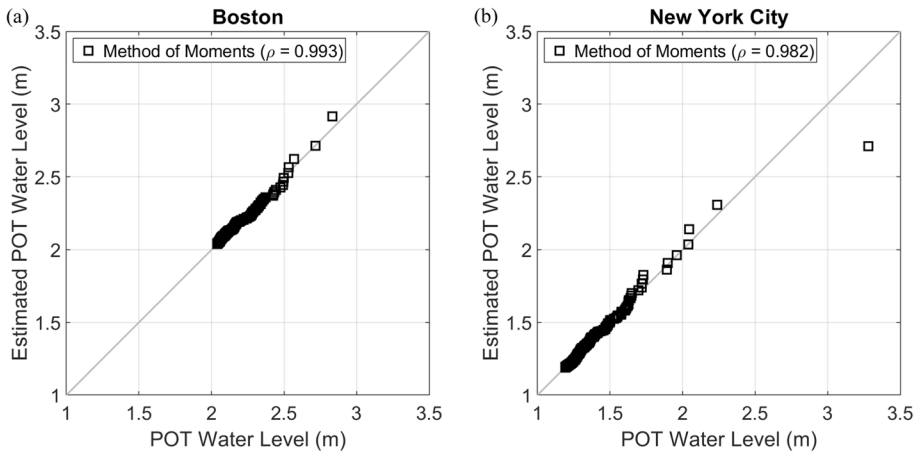
Fig. 5 Quantile–quantile plots for the detrended POT water levels. **a** Boston and **b** New York City

three projections are developed for low, intermediate, and high greenhouse gas emission scenarios, corresponding to representative concentration pathways (RCPs) of 2.6, 4.5, and 8.5, respectively. RCPs 2.6, 4.5, and 8.5 describe three twenty-first century pathways of greenhouse gas emissions and atmospheric concentrations, air pollutant emissions, and land use (IPCC 2014). Note that the sea level trend projections estimated by Kopp et al. (2014) are presented as the sea level changes in 2030, 2050, 2100, 2150, and 2200 with respect to the sea level in 2000. In this paper, the sea level in 2000 is obtained by the SLR trend estimated using Eq. (1). As a user-defined parameter, the future time span is selected to be the current year through 2200, which is consistent with Kopp et al. (2014). Figure 6 shows these sea level trend projections.

Regardless of the method used to project sea level trends, the projection always exhibits uncertainty. For sea level trend projections estimated by Kopp et al. (2014), the uncertainty is presented as the estimation's 2.5th–97.5th percentile, calculated using local sea level probability distributions. As mentioned in Kopp et al. (2014), local sea level probability distributions are calculated using samples from time-dependent probability distributions of cumulative contributions to sea level rise for each of the individual components (i.e., ice sheet components, glacier and ice cap, global mean thermal expansion and regional ocean steric and dynamic effects, land water storage, and long-term, local, nonclimatic sea level change due to factors such as glacial isostatic adjustment, sediment compaction, and tectonics). The uncertainty of sea level trend projections is shown in Fig. 6 as shaded areas.

3.4 Flood hazard curves

In this section, two RPs are used to develop flood hazard curves under different sea level trend projections with uncertainty. The developed flood hazard curves can be used to define the design flood level, estimate the performance of structures under coastal flooding, and assess community resilience.
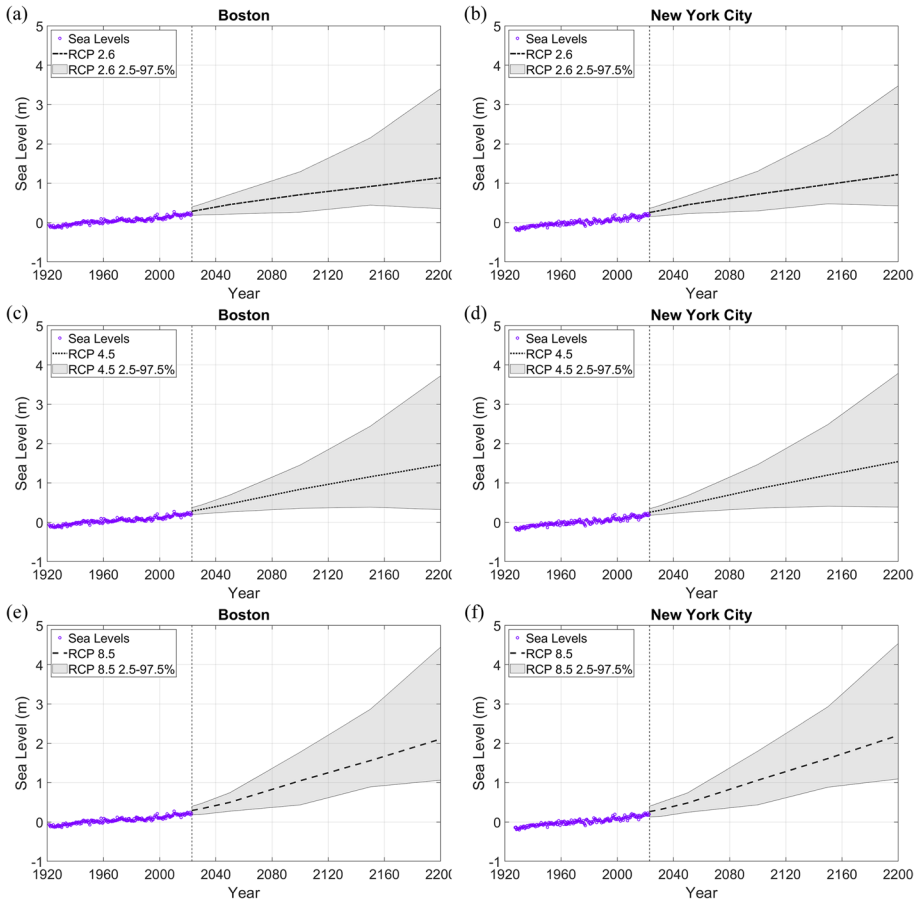
Fig. 6 Sea level trend projections with uncertainty estimated by Kopp et al. (2014) for three greenhouse gas emission scenarios (shown as RCP) with corresponding 2.5th–97.5th percentile intervals for Boston (left column) and New York City (right column); **a**, **b** RCP 2.6, **c**, **d** RCP 4.5, and **e**, **f** RCP 8.5

3.4.1 A retrospective comparison with other studies and historical flood events

Figure 7 shows the flood hazard curves developed under projected sea level trends for three greenhouse gas emission scenarios estimated by Kopp et al. (2014). For comparison purposes, the flood hazard curves under ST conditions and those developed by extrapolating the estimated SLR trend (see Fig. 2) are also shown in Fig. 7. The flood hazard curves in this paper, which can support conclusions about future RPs, are compared with other studies that report either the 100-year water level or the RP corresponding to a particular event. Under ST conditions, the 100-year water levels reported by other studies are shown in Fig. 7 to be compared with the developed ST flood hazard curves. Under NS conditions, however, no direct comparison is available. Because there are no previous studies incorporating RPs in an NS context to perform frequency analysis for Boston and New York City.

For the Boston case, the 100-year water levels estimated by FEMA (2016) and Nadal-Caraballo et al. (2016) are slightly lower than the ones estimated by the ST flood hazard curves in this paper (see Fig. 7a and c). This is primarily because (1) FEMA (2016) used
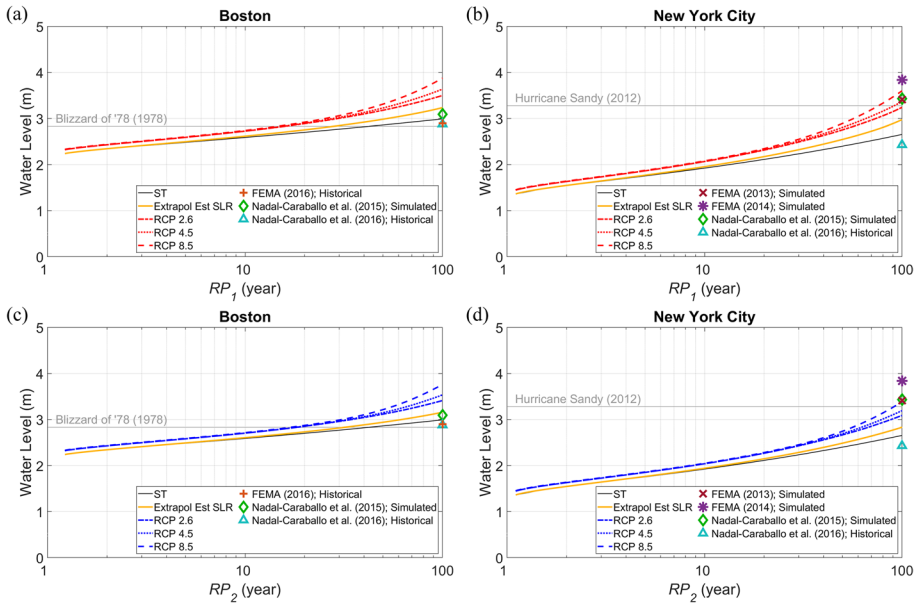
Fig. 7 Flood hazard curves developed under different sea level trend projections (stationary, extrapolating the estimated SLR trend, and three greenhouse gas emission scenarios estimated by Kopp et al. (2014)) compared with other studies and historical flood events for Boston (left column) and New York City (right column) interpreted using **a**, **b** RP_1 and **c**, **d** RP_2

historical water level data for frequency analysis without considering sea level trend, and (2) Nadal-Caraballo et al. (2016) used different water level data (hourly water levels and monthly maximum water levels) for sea level trend estimation. As compared with Nadal-Caraballo et al. (2015), the 100-year water level estimated by the ST flood hazard curve is lower, with a relative difference of 3% (see Fig. 7a and c). This is because Nadal-Caraballo et al. (2015) used water level data derived from thousands of simulated storms obtained by storm surge models instead of using historical water level data. As expected, in comparison with thousands of simulated storms, the historical record is relatively minimal and includes fewer extreme storm occurrences, resulting in limited water level data for hazard analysis.

For the New York City case, a result similar to that of the Boston case is observed (see Fig. 7b and d). The 100-year water level estimated by Nadal-Caraballo et al. (2016), which used historical water level data, is lower than the one derived using the ST flood hazard curve. Conversely, the 100-year water levels estimated using data from thousands of simulated storms (FEMA 2014; Nadal-Caraballo et al. 2015) and hundreds of simulated storms (FEMA 2013) are higher than the ones derived using the ST flood hazard curve. The corresponding relative differences vary from 29 to 45%, which are much larger than the 3% relative difference resulting from Nadal-Caraballo et al. (2015) for the Boston case. The main reason for this discrepancy is the different geographical locations. Compared with Boston, New York City has a lower latitude (see Table 1), which indicates that New York City is more easily hit by tropical cyclones (e.g., Hurricane Sandy 2012). Tropical cyclones tend to produce higher surge than extratropical cyclones (e.g., Blizzard of'78 1978) since they typically exhibit higher intensity (Nadal-Caraballo et al. 2015). Considering that most simulated storms developed by FEMA (2013), FEMA (2014), and Nadal-Caraballo et al. (2015) are tropical cyclones, the resulting water levels could have more extreme values,

compared with the Boston case. Also, the historical record has limited water level data and relatively sparse extreme storm occurrences. Therefore, the 100-year water levels estimated by FEMA (2013), FEMA (2014), and Nadal-Caraballo et al. (2015) are much higher than the one derived using the ST flood hazard curve and close to the water levels from NS flood hazard curves.

The historical flood events that resulted in the highest water levels–Blizzard of'78 (1978) for Boston and Hurricane Sandy (2012) for New York City–are shown in Fig. 7. For ease of comparison, the RPs for these two events obtained by the flood hazard curves under different sea level trend projections are shown in Table 3. For both the Boston and New York City cases, the RPs decrease as the slope of the sea level trend projections increases (see Fig. 6). It can be concluded that the use of this paper's approach to NS frequency analysis can lead to considerably lower estimations of historical flood event RPs.

The highest water levels are outliers that affect the trend of POT water levels, the probability distribution of POT water levels, and, in turn, the flood hazard curves (see Figs. 4, 5, and 7). If Hurricane Sandy had hit Boston at high tide, which is 5.5 h earlier than it did, a 3-m storm surge could have been recorded (CBS New Boston 2012), and more than 6% of Boston would have been underwater (Loth 2013; Friedman et al. 2019). This would have resulted in a water level higher than the one caused by the Blizzard of'78 and would have affected the behavior of the flood hazard curve developed here. As such, if a Hurricane Sandy-level event were to hit Boston at high tide, the flood hazard curves shown in Fig. 7 would likely be underestimated. Considering the time interval between high tide and storm surge can affect water level, an alternative NS frequency analysis can be performed focusing on storm surges, as opposite to the water levels discussed in this paper. The storm surges can be obtained by removing the astronomical tide heights from the historical water levels. The probability distribution of detrended storm surges can be modeled using the proposed methodology and incorporated with different tidal levels and sea level trend projections. Compared with the flood hazard curves shown in Fig. 7, the resulting flood hazard curves can account for the effect due to storm landfall time.

In terms of the different interpretations of RP, both RP_1 and RP_2 are used for developing flood hazard curves in an NS context (Olsen et al. 1998; Cooley 2013; Obeysekera and Salas 2014; Read and Vogel 2015). As shown in Table 3, RP_2 is larger than RP_1 for a given water level. In other words, the water level estimated using RP_1 is higher than the one estimated using RP_2. Similar observations are reported by Olsen et al. (1998) and Read and Vogel (2015). While, the RP_1 value results in a more conservative water level estimation, it requires that the trends to be indefinitely extrapolated. The RP_2 calculation, however, requires extrapolation only over the RP_2 years, and therefore it is considered a more suitable choice.

3.4.2 Uncertainty of flood hazard curves

The uncertainty of flood hazard curves arises from two sources: probability distributions of POT water levels and sea level trend projections. As discussed above, it is reasonable to assume that the probability distribution of future POT water levels is constant. Therefore, the uncertainty arising from the probability distributions of POT water levels is not included in this paper. Only the uncertainty arising from sea level trend projections is considered (see Fig. 6). The uncertainty of the flood hazard curves is quantified by the same statistical interval as the uncertainty of the sea level trend projections and is shown in Figs. 8 and 9 as shaded areas.

Table 3 RPs for historical events estimated by the flood hazard curves developed using different sea level trend projections

Location	Historical flood event	Water level (m)	RP (year)	Sea level trend projection				
				ST	Extrapolating the estimated SLR	RCP 2.6	RCP 4.5	RCP 8.5
Boston	Blizzard of'78	2.83	RP_1;	43	28	16	16	15
			RP_2;	43	32	18	18	17
New York City	Hurricane Sandy	3.28	RP_1;	399	131	104	91	76
			RP_2;	399	191	128	110	91

Fig. 8 Flood hazard curves with uncertainty interpreted using RP_1 under sea level trend projections (shown as RCP) estimated by Kopp et al. (2014) for Boston (left column) and New York City (right column) **a**, **b** RCP 2.6, **c**, **d** RCP 4.5, and **e**, **f** RCP 8.5

4 Conclusions

A straightforward approach for NS coastal flood frequency analysis is presented to address two important issues: (1) sea level trend projections that do not incorporate in frequency analysis and (2) the impact of NS behavior on the widely used RP concept. This NS coastal flood hazard analysis can be conducted in four main steps: (1) estimating SLR to detrend water level data, (2) fitting probability distributions to POT water levels, (3) incorporating the existing sea level trend projections in RP calculations, and (4) describing the NS behavior of RPs (RP_1 and RP_2). The final result is flood hazard curves with uncertainty that describe the probabilistic behavior of future coastal water levels.

Two case studies are conducted, one for Boston and one for New York City. The results demonstrate that, compared with frequency analysis under ST conditions, the use of this NS coastal flood frequency analysis can lead to considerably lower estimates of the RPs
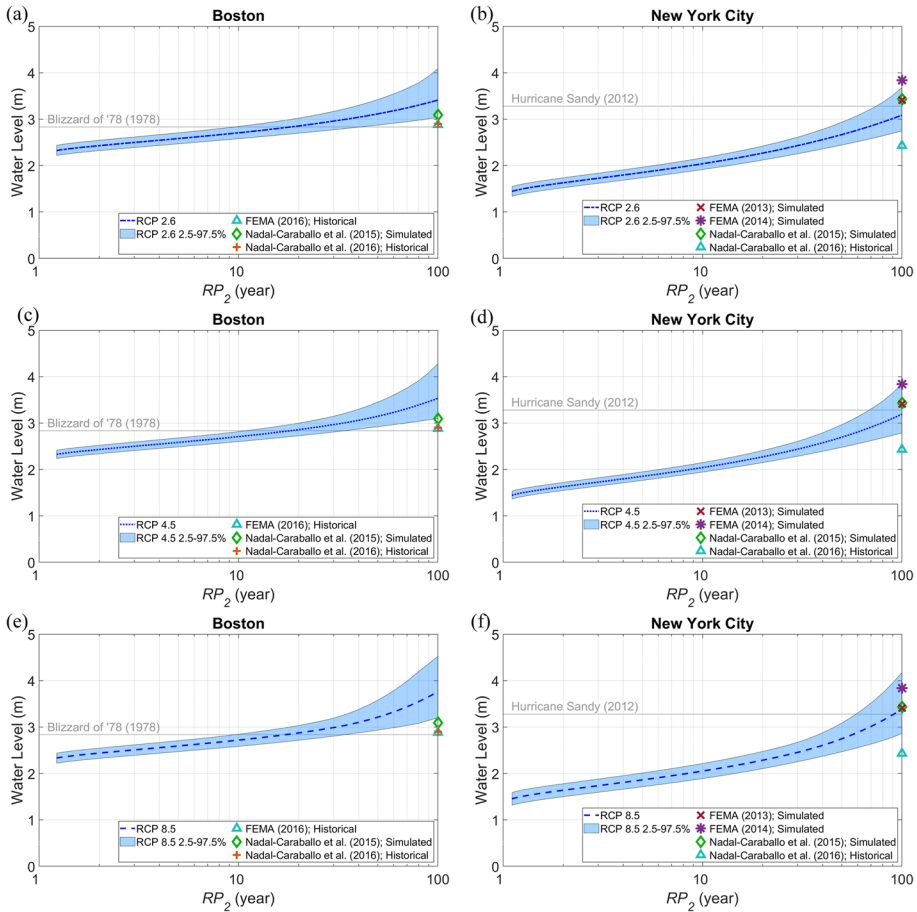
Fig. 9 Flood hazard curves with uncertainty interpreted using RP_2 under sea level trend projections (shown as RCP) estimated by Kopp et al. (2014) for Boston (left column) and New York City (right column) **a**, **b** RCP 2.6, **c**, **d** RCP 4.5, and **e**, **f** RCP 8.5

posed by historical flood events. The comparison between the two interpretations of RPs shows that, for a given water level, RP_2 is larger than RP_1.

Notable advantages of this NS coastal flood frequency analysis include.

(1) As opposed to extrapolating the estimated SLR trend, which is based on a purely statistical approach, sea level trend projections that model various future climate change scenarios with physical bases (e.g., greenhouse gas emissions scenarios in Kopp et al. 2014) are used in the development of flood hazard curves. This can provide users with a better understanding of the probabilistic behavior of future coastal flood events under climate change.

(2) Two interpretations of RP (RP_1 and RP_2) are evaluated in an NS context. Both RP_1 and RP_2 are well suited to the development of flood hazard curves. Normally, flood hazard curves do not include RPs in an NS context and, thus, are representative of only a par-

Table 4 Shapiro–Wilk test (Shapiro and Wilk 1965) results for ε'

Location	p-value	Diagnostic result
Boston	0.671	Normality is NOT rejected
New York City	0.396	Normality is NOT rejected

Table 5 Breusch-Pagan test (Breusch and Pagen 1979) results for ε'

Location	p-value	Diagnostic result
Boston	0.245	Homoscedasticity is NOT rejected
New York City	0.053	Homoscedasticity is NOT rejected

ticular moment in time. In contrast, engineers can use the flood hazard curves presented in this paper in conjunction with a planning horizon for coastal infrastructure design, evaluation of infrastructure performance, and community resilience assessment.

(3) This NS coastal flood frequency analysis is a user-friendly approach for engineers because advanced training in statistics is not needed to perform it. This approach can be applied to any city with sufficient historical water level data and extended to other hazard measures (e.g., streamflow, precipitation).

(4) The improvements derived from this NS coastal flood frequency analysis include a method to account for the uncertainty of probability distributions of POT water levels and the estimation of sea level trend projections that combine historical water levels with various climate change scenarios.

Appendix

Regression residual analysis

The normality of regression residuals in Eq. (3), ε', is evaluated using Shapiro–Wilk test (Shapiro and Wilk 1965). The test results are shown in Table 4. For Boston and New York City cases, the obtained p-values are larger than 0.05. It indicates that the null hypothesis that ε' are normal is not rejected.

The homoscedasticity of ε' is evaluated using Breusch-Pagan test (Breusch and Pagen 1979). The test results are shown in Table 5. For Boston and New York City cases, the obtained p-values are larger than 0.05. It indicates that the null hypothesis that ε' are homoscedastic is not rejected.

Figure 10 shows the lags of serial correlation coefficient of ε' along with 95% confidence intervals. Since, most data points fall between 95% confidence intervals, it is reasonable to assume that ε' are independent (no serial correlation).
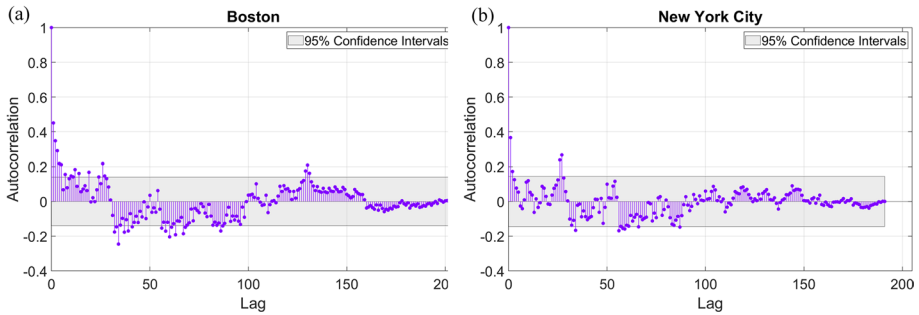
Fig. 10 Correlogram of ε' along with 95% confidence intervals. **a** Boston and **b** New York City
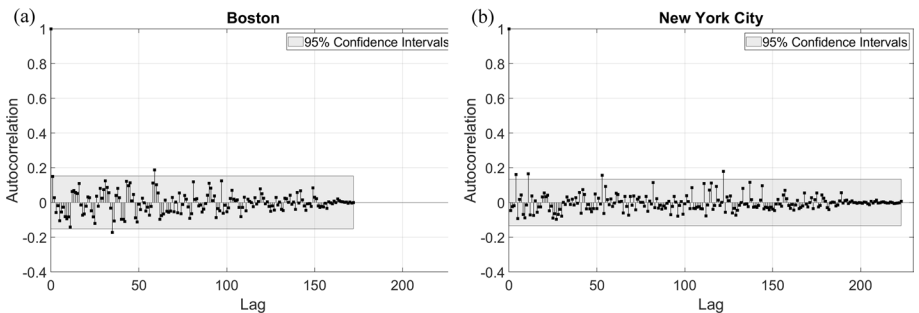

Fig. 11 Correlogram of POT water levels along with 95% confidence intervals. **a** Boston and **b** New York City

Independence of peak-over-threshold water levels

Figure 11 shows the lags of serial correlation coefficient of the POT water levels along with 95% confidence intervals. Most data points fall between 95% confidence intervals, which indicates that the independence condition of POT water levels is met.

Declarations

Conflict of interest The authors have no relevant financial or nonfinancial interests to disclose.

References

Baldan D, Coraci E, Crosato F, Ferda M, Bonometto A, Morucci S (2022) Importance of non-stationary analysis for assessing extreme sea levels under sea level rise. Nat Hazard 22(11):3663–3677

Bezak N, Brilly M, Šraj M (2014) Comparison between the peaks-over-threshold method and the annual maximum method for flood frequency analysis. Hydrol Sci J 59(5):959–977

Bommier E (2014) Peak-over-threshold modelling of environmental data. Project Report, Department of Mathematics, Uppsala University, Sweden

Breusch TS, Pagan AR (1979) A simple test for heteroscedasticity and random coefficient variation. Econometrica 47(5):1287–1294

Cazenave A, Llovel W (2010) Contemporary sea level rise. Ann Rev Mar Sci 2(1):145–173

CBS News Boston (2012) "What if Hurricane Sandy hit Boston?" CBS News. https://www.cbsnews.com/boston/news/what-if-hurricane-sandy-hit-boston/. Accessed 20 Sept 2023

Cheng L, AghaKouchak A, Gilleland E, Katz RW (2014) Non-stationary extreme value analysis in a changing climate. Clim Change 127(2):353–369

Church JA, White NJ (2006) A 20th century acceleration in global sea-level rise. Geophys Res Lett 33(1):L01602

Coles S (2001) An introduction to statistical modeling of extreme values. Springer, New York

Cooley D (2013) Return periods and return levels under climate change. In: AghaKouchak A, Easterling D, Hsu K, Schubert S, Sorooshian S (eds) Extremes in a changing climate: detection, analysis and uncertainty. Springer, Dordrecht, Netherlands

Davison AC, Smith RL (1990) Models of exceedances over high thresholds. J Royal Stat Soc Series b, Methodol 52(3):393–442

Eastoe EF, Tawn JA (2010) Statistical models for overdispersion in the frequency of peaks over threshold data for a flow series. Water Resource Res 46(2):W02510

FEMA (2007) Atlantic Ocean and Gulf of Mexico coastal guidelines update. FEMA, Washington, DC

FEMA (2013) Flood insurance study City of New York, New York. FEMA, Washington, DC

FEMA (2014) Region II storm surge project – Joint probability analysis of hurricane and extratropical flood hazards. FEMA, Washington, DC

FEMA (2016) Flood insurance study Suffolk County, Massachusetts (all jurisdictions). FEMA, Washington, DC

Friedman E, Breitzer R, Solecki W (2019) Communicating extreme event policy windows: discourses on Hurricane Sandy and policy change in Boston and New York City. Environ Sci Policy 100:55–65

Ghanbari M, Arabi M, Obeysekera J, Sweet W (2019) A coherent statistical model for coastal flood frequency analysis under nonstationary sea level conditions. Earth's Future 7(2):162–177

Ghanbari M, Arabi M, Kao S-C, Obeysekera J, Sweet W (2021) Climate change and changes in compound coastal-riverine flooding hazard along the US coasts. Earth's Future 9(5):e2021EF002055

Goddard PB, Yin J, Griffies SM, Zhang S (2015) An extreme event of sea-level rise along the Northeast coast of North America in 2009–2010. Nat Commun 6(1):6346

Gringorten II (1963) A plotting rule for extreme probability paper. J Geophys Res 68(3):813–814

Hall JA, Gill S, Obeysekera J, Sweet W, Knuuti K, Marburger J (2016) Regional sea level scenarios for coastal risk management: Managing the uncertainty of future sea level change and extreme water levels for Department of Defense coastal sites worldwide. U.S. Department of Defense, Strategic Environmental Research and Development Program, Alexandria, VA

Hay CC, Morrow E, Kopp RE, Mitrovica JX (2015) Probabilistic reanalysis of twentieth-century sea-level rise. Nature (london) 517(7535):481–484

Hecht JS, Vogel RM (2020) Updating urban design floods for changes in central tendency and variability using regression. Adv Water Res 136:103484

Hecht JS, Barth NA, Ryberg KR, Gregory AE, Elsevier BV (2022) Simulation experiments comparing non-stationary design-flood adjustments based on observed annual peak flows in the conterminous United States. J Hydrol 17:100115

Helsel DR, Hirsch RM, Ryberg KR, Archfiend SA, Gilroy EJ (2020) Statistical methods in water resources: Techniques and methods 4-A3. U.S. Department of the Interior, U.S. Geological Survey, Reston, VA

Hosking JRM, Wallis JR (1987) Parameter and quantile estimation for the generalized Pareto distribution. Technometrics 29(3):339–349

IPCC (2014) Climate change 2014: synthesis report. Contribution of working groups I, II and III to the fifth assessment report of the intergovernmental panel on climate change. Core Writing Team, Pachauri RK, Meyer LA (eds) Intergovernmental Panel on Climate Change, Geneva, Switzerland

Jia Y, Sasani M (2021) Modeling joint probability of wind and flood hazards in Boston. Nat Hazards Rev, ASCE 22(4):4021047

Joyner MD, Puentes B, Gardner C, Steinberg S, Sasani M (2022) Multiobjective optimization of building seismic design for resilience. J Struct Eng, ASCE 148(4):04022006

Katz RW, Parlange MB, Naveau P (2002) Statistics of extremes in hydrology. Adv Water Res 25(8–12):1287–1304

Katz RW (2013) Statistical methods for nonstationary extremes. In: AghaKouchak A, Easterling D, Hsu K, Schubert S, Sorooshian S (eds) Extremes in a changing climate: detection, analysis and uncertainty. Springer, Dordrecht, Netherlands

Kim S, Kho Y, Shin H, Heo J-H (2008) Derivation of the probability plot correlation coefficient test statistics for the generalized logistic and the generalized Pareto distributions. In: Proceedings of the World Environmental and Water Resources Congress. ASCE, Reston, VA

Kirshen P, Watson C, Douglas E, Gontz A, Lee J, Tian Y (2008) Coastal flooding in the Northeastern United States due to climate change. Mitig Adapt Strat Glob Change 13(5):437–451

Kopp RE, Horton RM, Little CM, Mitrovica JX, Oppenheimer M, Rasmussen DJ, Strauss BH, Tebaldi C (2014) Probabilistic 21st and 22nd century sea-level projections at a global network of tide-gauge sites. Earth's Future 2(8):383–406

Lang M, Ouarda TBMJ, Bobée B (1999) Towards operational guidelines for over-threshold modeling. J Hydrol 225(3):193–117

Loth R (2013) Boston prepares for future superstorms. The Boston Globe. https://www.bostonglobe.com/opinion/2013/02/23/boston-prepares-for-future-superstorms/07N63UN9uRmt8v73L1QIjO/story.html. Accessed 20 Sept 2023

Luke A, Vrugt JA, AghaKouchak A, Matthew R, Sanders BF (2017) Predicting nonstationary flood frequencies: evidence supports an updated stationarity thesis in the United States. Water Resour Res 53(7):5469–5494

Méndez FJ, Menéndez M, Luceño A, Losada IJ (2006) Estimation of the long-term variability of extreme significant wave height using a time-dependent peak over threshold (POT) model. J Geophys Res 111:C07014

Menéndez M, Woodworth PL (2010) Changes in extreme high water levels based on a quasi-global tide-gauge data set. J Geophys Res 115:C10011

Mudersbach C, Jensen J (2010) Nonstationary extreme value analysis of annual maximum water levels for designing coastal structures on the German North Sea coastline. J Flood Risk Manag 3(1):52–62

Nadal-Caraballo NC, Melby JA, Gonzalez VM (2016) Statistical analysis of historical extreme water levels for the U.S. North Atlantic coast using Monte Carlo life-cycle simulation. J Coastal Res 32(1):35–45

Nadal-Caraballo NC, Melby JA, Gonzalez VM, Cox AT (2015) *North Atlantic Coast Comprehensive Study—Coastal Storm Hazards from Virginia to Maine*. US Army Corps of Engineers, Engineer Research and Development Center, Coastal and Hydraulics Laboratory, Vicksburg, MS

Naseri K, Hummel MA (2022) A Bayesian copula-based nonstationary framework for compound flood risk assessment along US coastlines. J Hydrol 610:128005

Nicholls RJ, Cazenave A (2010) Sea-level rise and its impact on coastal zones. Sci (am Associat Adv Sci) 328(5985):1517–1520

NOAA (2023) Tides & Currents. https://tidesandcurrents.noaa.gov/. Accessed 24 Feb 2023

Obeysekera J, Park J (2013) Scenario-based projection of extreme sea level. J Coast Res 29(1):1–7

Obeysekera J, Salas JD (2014) Quantifying the uncertainty of design floods under nonstationary conditions. J Hydrol Eng, ASCE 19(7):1438–1446

Obeysekera J, Salas JD (2016) Frequency of recurrent extremes under nonstationarity. J Hydrol Eng, ASCE 21(5):04016005

Olsen JR, Lambert JH, Haimes YY (1998) Risk of extreme events under nonstationary conditions. Risk Anal 18(4):497–510

Pan X, Rahman A, Haddad K, Quarda TBMJ (2022) Peaks-over-threshold model in flood frequency analysis: a scoping review. Stoch Env Res Risk Assess 36(9):2419–2435

Parey S, Malek F, Laurent C, Dacunha-Castelle D (2007) Trends and climate evolution: Statistical approach for very high temperature in France. Clim Change 81(3):331–352

Parey S, Hoang TTH, Dacunha-Castelle D (2010) Different ways to compute temperature return levels in the climate change context. Environmetrics 21(7–8):698–718

Parris A, Bromirski P, Burkett V, Cayan D, Culver M, Hall J, Horton R, Knuuti K, Moss R, Obeysekera J, Sallenger A, Weiss J (2012) Global sea level rise scenarios for the US national climate assessment. NOAA Tech Memo OAR CPO-1

Razmi A, Golian S, Zahmatkesh Z (2017) Non-stationary frequency analysis of extreme water level: application of annual maximum series and peak-over threshold approaches. Water Resour Manage 31(7):2065–2083

Read LK, Vogel RM (2015) Reliability, return periods, and risk under nonstationarity. Water Resour Res 51(8):6381–6398

Salas JD, Obeysekera J (2014) Revisiting the concepts of return period and risk for nonstationary hydrologic extreme events. J Hydrol Eng, ASCE 19(3):554–568

Salas JD, Obeysekera J, Vogel RM (2018) Techniques for assessing water infrastructure for nonstationary extreme events: a review. Hydrol Sci J 63(3):325–352

Serago JM, Vogel RM (2018) Parsimonious nonstationary flood frequency analysis. Adv Water Res 122:1–16

Shapiro SS, Wilk MB (1965) An analysis of variance test for normality (complete samples). Biometrika 52(3–4):591–611

Silva AT, Portela MM, Naghettini M (2014) On peaks-over-threshold modeling of floods with zero-inflated poisson arrivals under stationarity and nonstationarity. Stoch Env Res Risk Assess 28(6):1587–1599

Stedinger J, Vogel RM, Foufoula-Georgiou E (1993) Frequency analysis of extreme events. In: Maidment DR (eds) Handbook of Hydrology. McGraw-Hill, New York

Sweet WV, Park J, Marra JJ, Zervas C, Gill S (2014) Sea level rise and nuisance flood frequency changes around the United States. NOAA Technical Report NOS CO-OPS 073. National Oceanic and Atmospheric Administration, National Ocean Service, Silver Spring, MD

Sweet WV, Kopp RE, Weaver CP, Obeysekera J, Horton RM, Thieler ER, Zervas C (2017) Global and regional sea level rise scenarios for the United States. Silver Spring, MD: NOAA Technical Report NOS CO-OPS 083. National Oceanic and Atmospheric Administration, National Ocean Service. Silver Spring, MD

Sweet WV. Hamlington BD, Kopp RE, Weaver CP, Barnard PL, Bekaert D, Brooks W, Craghan M, Dusek G, Frederikse T, Garner G, Genz AS, Krasting JP, Larour E, Marcy D, Marra JJ, Obeysekera J, Osler M, Pendleton M, Roman D, Schmied L, Veatch W, White KD, Zuzak C (2022) Global and regional sea level rise scenarios for the United States: Updated mean projections and extreme water level probabilities along U.S. Coastlines. NOAA Technical Report NOS 01. National Oceanic and Atmospheric Administration, National Ocean Service, Silver Spring, MD

Tabari H (2021) Extreme value analysis dilemma for climate change impact assessment on global flood and extreme precipitation. J Hydrol 593:125932

Taherkhani M, Vitousek S, Barnard PL, Frazer N, Anderson TR, Fletcher CH (2020) Sea-level rise exponentially increases coastal flood frequency. Sci Rep 10(1):6466

Talke SA, Kemp AC, Woodruff J (2018) Relative sea level, tides, and extreme water levels in Boston Harbor from 1825 to 2018. J Geophys Res: Oceans 123(6):3895–3914

Tebaldi C, Strauss BH, Zervas CE (2012) Modelling sea level rise impacts on storm surge along US coasts. Environ Res Lett 7(1):14032

Tebaldi C, Ranasinghe R, Vousdoukas M, Rasmussen DJ, Vega-Westhoff B, Kirezci E, Kopp RE, Sriver R, Mentaschi L (2021) Extreme sea levels at different global warming levels. Nat Clim Chang 11(9):746–751

Theil H (1950) A rank-invariant method of linear and polynomial regression analysis, I, II, and III. In: Proceedings of the Royal Netherlands Academy of Sciences, 53:386–392, 521–525, 1397–1412

Vitousek S, Barnard PL, Fletcher CH, Frazer N, Erikson L, Storlazzi CD (2016) Doubling of coastal flooding frequency within decades due to sea-level rise. Sci Rep 7(1):1399

Yin J, Schlesinger ME, Stouffer RJ (2009) Model projections of rapid sea-level rise on the northeast coast of the United States. Nat Geosci 2(4):262–266

Zervas C (2013) Extreme water levels of the United States 1893–2010. U.S. Department of Commerce, National Oceanic and Atmospheric Administration, National Ocean Service, Center for Operational Oceanographic Products and Services, Silver Spring, MD

Zwillinger D (2012) CRC standard mathematical tables and formulae, 32nd edn. CRC Press, Boca Raton, FL

Publisher's Note Springer Nature remains neutral with regard to jurisdictional claims in published maps and institutional affiliations.